Technical Note	LIGO-T2200178–	2022/10/31

2022 LIGO SURF Final Report: Emissivity Engineering for Radiative CryoCooling

Clare Nelle; Mentors: Rana Adhikari, Radhika Bhatt, Christopher Wipf

Contents

1   Abstract

The Laser Interferometer Gravitational Wave Observatory (LIGO) will undergo the cryogenic Voyager upgrade to increase detector sensitivity, allowing gravitational wave astronomers to learn more information about astronomical events in the field of multimessenger astrophysics. This upgrade will require efficient cooling of the test mass, in part through high thermal emissivity coatings applied to the barrel surface. We used Markov Chain Monte Carlo (MCMC) analysis to build an accurate model of the cryostat system and to fit the test mass emissivity value to noisy data from the system cooldown. These results showed that the cryostat system used was both radiatively and conductively cooled. We found that the emissivity of a silicon wafer was 0.72 +/- .04, showing that the cleaning method was insufficient for this sample. This analysis will be applied to emissivity tests of various high thermal emissivity coatings that potentially can be used in the LIGO Voyager upgrade.

2   Background

Since the LIGO-VIRGO Scientific Collaboration's detection of gravitational waves in 2016, the field of gravitational wave astronomy has allowed for new ways to observe physical phenomena. Collaborators hope to refine the precision of LIGO detection with further Advanced LIGO upgrades to explore new avenues in gravitational wave astronomy and multimessenger astrophysics. The LIGO Voyager version is an upgrade that will increase the detector sensitivity to about 700-1100 Mpc [1] by using cryogenic temperatures of 123 K to reduce thermal noise within the LIGO barrel. It is important for the test mass to be cooled to 123 K because it is at this value where the coefficient of thermal expansion for silicon is zero. Mariner is a cryogenic and suspensions upgrade to the LIGO 40 Meter Laboratory at Caltech, which is a Voyager upgrade prototype. The Mariner upgrade will help prepare and troubleshoot for the Voyager upgrade at the LIGO observatory locations.

Constacio et. al. found that silicon has a high enough natural emissivity to maintain the temperature of test masses at 123K, meaning that it is an appropriate material to use in the Voyager upgrade barrel [2]. However, because the LIGO interferometer lasers must be very powerful (around 10W), Constacio et. al. theorized that the barrel will also require a high thermal emissivity to increase radiative coupling to its cooled environment. This will improve the cool-down time of the Voyager upgrade apparatus and help maintain the system at 123 K despite the excess heating from the laser [2].

It is important to test the emissivities of various materials to identify coatings that will sufficiently increase coupling with the cold surrounding environment, helping to offset the excess heating from the interferometer laser. The coatings will need to have emissivity that will absorb radiation between 10 - 100 um wavelength [3]. This will reduce the cool-down time of the system and allow for conditions to hold the system at 123K.

To determine the emissivities of various black coatings, the cool-down curves from room temperature to 123 K is monitored with respect to time using thermocouple thermometers for test masses in a cryostat chamber (called Megastat) at vacuum. Then, the emissivity value and uncertainty can be extracted from these data by plotting emissivity against tem-

perature [2]. By implementing a Markov-Chain Monte Carlo (MCMC) analysis script, it is possible to extract the emissivity of the test mass. MCMC also allows us to define some of the parameters describing the cryostat system. This script can be applied to emissivity tests for many black coatings that can potentially be used in the LIGO Mariner and Voyager upgrades.

The emissivity of a silicon wafer test mass was successfully extracted from cooldown data using MCMC analysis. Additionally, the size of the heat leaks in the cryostat enclosure and the magnitude of conductive cooling was measured well with uncertainty. The analysis also showed that the emissivity of the inner and outer shield of the cryostat did not have a significant effect on the result, meaning that the small chips in the high emissivity coating of the testing chamber would not effect the emissivity estimation results.

2.1 Heat Transfer

Heat transfer via conduction and radiation can be modeled using differential equations derived from the equation for specific heat capacity $Q = mc_p\Delta T$ (Equation 1) where Q is the energy of an object in Joules, m is the mass in kg, c_p is the specific heat capacity in units of $J * kg^{-1} * K^{-1}$, and ΔT is the relative change in temperature of the object. This equation relates the amount of energy needed to change temperature of an object, given a mass and the heat capacity of the substance. Taking the first derivative of this equation with respect to time gives

$$\frac{dQ}{dt} = mc_p\frac{dT}{dt}$$

(Equation 2) relating a power (left hand side) in Js^{-1} to a change in temperature with respect to time in Ks^{-1}. By isolating the $\frac{dT}{dt}$ term, Equation 2 gives a differential equation that relates what power is necessary for a change in temperature of a object with respect to time.

Conductive heat transfer through a rod can be similarly modeled as

$$mc_p\frac{dT_1}{dt} = \frac{c_pA}{l}(T_2 - T_1)$$

(Equation 3) where A is the cross-sectional area of the rod and l is the length of the rod. This differential equation models how the change in temperature with respect to time of one end of the rod (T_1) is related to relative difference in temperature of the other end ($T_2 - T_1$).

The equation for radiative heat transfer is a nonlinear differential equation relating a time derivative to the difference in the fourth powers of the temperatures of two bodies that are radiatively coupled. Equation 4 describes this relation

$$mc_p\frac{dT_1}{dt} = \frac{\sigma(T_2^4 - T_1^4)}{R_1 + R_2 + R_3}$$

(Equation 4) where R_1, R_2, R_3 are resistive values (analogous to Ohm's law) describing how the surfaces emit and absorb radiation depending on how the two surfaces are geometrically oriented. The quantities R_1 and R_3 encode information about the thermal emissivites of the two surfaces. Emissivity is a dimensionless quantity from 0 to 1 that describes the ratio of

the amount of radiation that leaves a surface compared to that of a blackbody at the same temperature. Emissivity is a temperature-dependent function, although it is often reported as a constant.

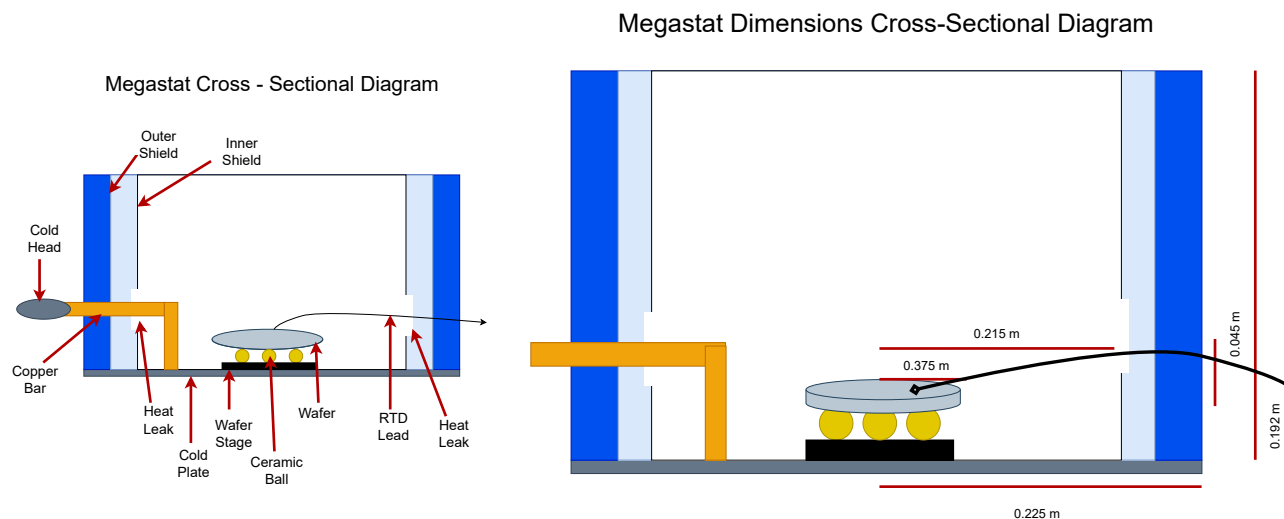## 2.2 Cryostat and Experimental Design

Figure 1: *Left:* A cross sectional diagram of the cryostat. Notice that there are multiple heat leaks in the cryostat inner shield. (Not to scale). *Right:* The cryostat dimensions used in the MCMC simulation. The distances from the center of the wafer to the heat leak and from the top of the wafer to the center of the test mass are used in the geometric view factor calculation.

To find the emissivity of the silicon wafer, cooldown temperature data was collected with respect to time. These data were obtained by monitoring the temperature of the silicon test mass placed in a cryostat using three resistance temperature detectors (RTDs) varnished to the test mass, the outer shield and the inner shield of the cryostat system (Figure 1) from the start of the cooldown to some arbitrary time after the temperature of the wafer, inner shield, and outer shield had stabilized.

This system, called Megastat, is conductivity cooled to about 51 K though a conductively contacted copper bar that is clamped to a cold head. The copper bar is in conductive contact with the floor of the chamber, or the cold plate (Figure 1). The cold plate is conductively contacted to the inner shield and the wafer mounting stage (note: this stage is to be removed). As a temporary measure while Megastat is under construction, two aluminum foil sheets painted with Aquadag, a high emissivity coating, were placed directly onto the cold plate. This increases the emissivity of the surrounding environment for faster cooldowns of Megastat while a new high emissivity cold plate is in construction. The inside of the inner shield was also painted with Aquadag coating, creating a high emissivity enclosure for the test mass cooldown. The environment can be approximated assuming that all of the radiation from the test mass will strike the enclosure walls.

Although Megastat is a close to perfect enclosure, there are two known heat leaks in the inner shield. Radiative heat transfer occurs between the test mass and outer shield through

the heat leaks. There is also conductive heat transfer through the RTD lead attached to the RTD that is varnished to the test mass. This lead is exposed to the outer shield as well, and had a non-negligible effect on the cooldown of the wafer, modeled by Equation 3. Finally, conductive cooling occurs through the ceramic ball bearings supporting the wafer as intermediaries between the mounting stage and the wafer, because of their high thermal resistance. Although these points of contact are very small and the thermal insulating properties of the ceramic balls are high, non-negligible conduction still occurs through these points. In the future, a new stage will be implemented to the cryostat design and the ceramic bearings will not be necessary.

This design was chosen for Megastat because it allows for faster cooldowns and more control over modeling the system. By making a chamber that encloses the wafer, it is possible to assume that nearly all of the radiation (except for the heat leak) leaving the wafer is absorbed by the inner shield, leading to some useful approximations in the model.

2.2.1 Net Heat Transfer Model

Megastat can be modeled using a four-term nonlinear differential equation describing the radiative heating, radiative cooling, conductive heating, and conductive cooling of the wafer. Equation 5 describes the net heat transfer of the system with respect to the wafer.

Variable	Meaning	Approximate Value
A_{tm}	Surface area of the test mass	0.0091 m^2
A_{is}	Surface area of the inner shield and enclosure	0.59 m^2
A_{hl}	Surface area of heat leak	.0009 m^2
α	Conductive cooling coefficient	n/a
β	Conductive heating coefficient	n/a
c_p	Specific heat capacity (silicon)	0.71 J/(g*K)
E_{is}	Emissivity of inner shield	0.9
E_{os}	Emissivity of outer shield	0.1
E_{tm}	Emissivity of test mass	0.7
$F_{(tm \to hl)}$	View factor between test mass and heat leak	n/a
m	Mass of testmass	.082 kg
σ	Stephen Boltzman Constant	5.67e-8 W*m$^{(-2)}$*K$^{(-4)}$
T_{tm}	Temperature of testmass	n/a
T_{is}	Temperature of inner shield	n/a
T_{os}	Temperature of outer shield	n/a
T_{amb}	Ambient temperature of the room	293 K

Figure 2: The variable names used to denote the Megastat system are defined above. Note: in the MCMC analysis, the emissivity of the test mass wafer, inner shield, and outer shield are defined as ϵ_1, ϵ_2 and ϵ_3 respectively.

$$mc_p\frac{dT_{tm}}{dt} = \frac{\sigma A_{tm}(T_{is}^4 - T_{tm}^4)}{\frac{1}{\epsilon_{tm}} + \frac{A_{tm}}{A_{is}}(\frac{1}{\epsilon_{is}} - 1)} + \frac{\sigma(T_{os}^4 - T_{tm}^4)}{\frac{1-\epsilon_{tm}}{A_{tm}\epsilon_{tm}} + \frac{1}{A_{tm}F_{tm->os}} + \frac{1-\epsilon_{os}}{A_{hl}\epsilon_{os}}} + \alpha(T_{is} - T_{tm}) + \beta(T_{amb} - T_{tm})$$

(Equation 5)

where variable names are referenced in Figure 2. It is easiest to Understand this equation by examining each term individually. The first term, describing the radiative cooling of the wafer, assumes that approximately all of the radiation from the test mass will be absorbed by the inner shield of the Megastat enclosure. This can be derived from the reciprocity relation,

$$F_{12}A_1 = F_{21}A_2$$

(Equation 6) where A_1 and A_2 are the surface areas of the radiatively coupled objects, and F_{12} and F_{21} represent the geometric view factors between the two surfaces. Equation 4 states that the ratios between the view factors and the surface areas are inversely related. In the case of Megastat, which describes a test mass enclosed by the inner shield, floor, and lid, the term F_{12} equals 1. This describes all of the radiation from the test mass (Surface 1) being absorbed by inner shield (Surface 2).

$$1A_1 = F_{21}A_2$$

Therefore, it is possible to write the view factor as the relationship between the ratio of the surface areas of the test mass and the enclosure:

$$\frac{A_1}{A_2} = F_{21}.$$

By plugging this term into the radiative cooling term (term 2) in Equation 5, this term becomes

$$\frac{\sigma A_{tm}(T_{is}^4 - T_{tm}^4)}{\frac{1}{\epsilon_{tm}} + \frac{A_{tm}}{A_{is}}(\frac{1}{\epsilon_{tm}} - 1)}.$$

This term encodes the emissivity of the test mass, which is the value that MCMC is extracting.

The radiative heating term can be described by

$$\frac{\sigma(T_{os}^4 - T_{tm}^4)}{\frac{1-\epsilon_{tm}}{A_{tm}\epsilon_{tm}} + \frac{1}{A_{tm}F_{tm->os}} + \frac{1-\epsilon_{os}}{A_{hl}\epsilon_{os}}}$$

The cryostat model for net radiative heat transfer is dependent on the geometric view factor, $F_{tm->os}$, of the test mass and the enclosure for the radiative terms. The geometric view factor is a quantity that describes the spatial orientation of two bodies that are radiatively coupled, described in more detail in section 3.2.1. In the case of the radiative cooling term, the view factor $F_{tm->is}$ is equal to 1 because all of the radiation from the test mass will be captured by the chamber (Figure 1). When considering the radiative heating term of the cryostat model, the size, shape, and relative orientation of the test mass and the heat leaks affects the amount of radiation that is absorbed by the test mass surface. In the second term of the net heat transfer equation (Equation 2), the geometric view factor is nonzero. It is also important to note that the radiative heating term is dependent on the temperature of the outer shield and not the temperature of the inner shield, as in the radiative cooling term.

There are two conductive terms for the conductive heating and cooling of the test mass. Conductive cooling can be approximated by the expression

$$\alpha(T_{is} - T_{tm})$$

and the conductive heating of the test mass as

$$\beta(T_{amb} - T_{tm})$$

Both of these terms are quantifying an amount of heating or cooling in the system, but are not accurately representing the geometry or size of the system. All of the coefficients and constants for these terms are combined into the α and β coefficients because nuances such as the cross-sectional area of the RTD leads or the size of the ceramic ball bearings is unnecessary to understand the cooldown curve of the wafer.

2.2.2 Markov Chain Monte Carlo Analysis

Markov Chain Monte Carlo analysis is a method of parameter estimation that uses Bayesian Statistics to develop posterior distributions based on information provided by the data and prior knowledge on the parameters. It is fundamentally related to Bayes theorem,

$$P(\theta|x) = \frac{P(x|\theta)P(\theta)}{P(x)}$$

(Equation 7) where θ is the parameter and x is the data. Bayes Theorem states that $P(\theta)$, or the prior knowledge of the distribution multiplied by $P(x|\theta)$, or the likelihood, is proportional the posterior distribution. The likelihood is the probability of the data given the parameter

MCMC for parameter estimation takes parameters in a vector space and fits different values of the indices to the model (Figure 3). The program explores a parameter space, maximizing the likelihood function in Equation 7 to return a posterior distribution of highest probability given the priors and the model. Figure 3 describes how MCMC finds the area of highest likelihood within a parameter space. MCMC defines "walkers" that start at some initial parameter vector provided by prior knowledge on the parameters. The walkers will evaluate the likelihood function at that position. For a defined number of steps, the walkers move to a new parameter vector and evaluate the likelihood function. If the likelihood of the new model is greater than the previous position, the walker will move to a new vector and repeat the process. If the likelihood is a worse match than the previous position, then the walker will move back the the previous position and try a new direction. This process is repeated with hundreds of walkers each independently exploring the parameter space.

MCMC will return a posterior distribution that is the product of the priors and the likelihood distribution. It has found the true parameters well when the posterior is a narrow, Gaussian distribution and the curve fit matches the data well. MCMC was not able to use the data to inform the values of the parameters when the posterior is unchanged from the prior distribution. For example, if uniform priors were passed to the function and uniform posteriors were returned, that means that the data could not inform a best fit for that parameter.

The python module emcee was used for parameter estimation of the emissivity of silicon. Emcee requires three helper functions to run: a function defining the prior distributions, the posterior distributions, and the likelihood. These functions are typically defined as the natural logarithm of these values because this means exponential quantities can be added instead of multiplied.

Emcee then handles all of the analysis. It was also useful to generate trace plots showing how the walkers explored the parameter space and then corner plots to visualize the posterior distributions and their degeneracy. Trace plots are a good way to check if the walkers are converging on a value of highest likelihood or if they are exploring the whole parameter space without convergence. Corner plots are the another way to see the results of the analysis.

2.3 Findings

The MCMC analysis of a silicon wafer test mass cooldown highlighted problems and intricacies with the current cryostat system, aiding in developing a more accurate model and better methods for future cooldowns for emissivity testing. In the process of fitting a model to the cooldown data, we found that a purely radiative model does not accurately represent the cryostat system and it was necessary to add conductive heating and cooling terms to the model. We also found that the emissivity of silicon was 0.72 +/- .04. However, this does not match the literature and therefore raised some questions on the preparation of the silicon wafer prior to the cool down, as well as understanding how high-emissivity debris within the cryostat affects cooldown data. We also found that although the emissivity of silicon is most likely temperature - dependent, the emissivity function with respect to temperature is not linear. With this information, we can theorize that there is a better non-linear fit for the temperature dependent emissivity of silicon. These findings will help us develop a better procedure for cleaning and preparing the cryostat and test mass for cooldowns, as well as providing some insight on how the emissivity of silicon changes as a function of temperature.
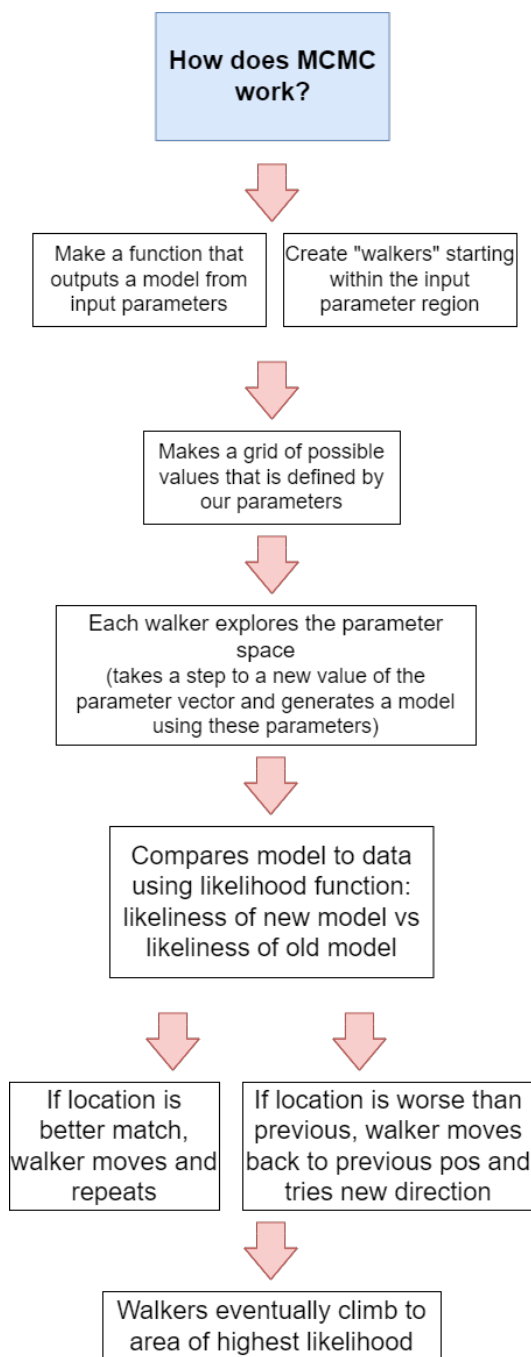

Figure 3: A qualitative understanding of the MCMC process helps build a foundation for understanding and implementing the emcee package.

3   Methods

3.1   Lab Work/Cryostat Cooldowns

3.1.1   RTD Calibration

In a previous cooldown, the RTD measuring the inner shield was returning colder temperatures than the RTD clamped to the cold head. This is physically impossible, leading the the belief that the RTDs were inaccurate relative to each other. This prompted re-calibration of the RTDs. For each RTD, the resistance was measured using a digital multimeter at the freezing point of water and at the boiling point of Nitrogen. From these two measurements, a linear fit line would give the temperature as a function of resistance for each RTD. Two measurements of the resistance across each RTD was measured. Only one measurement in the liquid nitrogen bath was used because the boiling point of nitrogen is much lower than room temperature, meaning that the temperature of the liquid nitrogen is known to high certainty. From initial observations, the RTD that was previously attached to the outer shield was reading a slightly higher resistance at the liquid nitrogen measurement than the other RTDs.

3.1.2   Preparing for Cooldowns

Before each Megastat cooldown, the wafer and chamber had to be properly prepared and cleaned. Based on observations and results from the summer cooldowns, the current procedure likely did not clean the wafer sufficiently. The current procedure was to wipe the wafer with acetone and then isopropanol alcohol using clean wipes until there was no visible debris on the wafer surface. For future cooldowns, the wafer will need to be more carefully cleaned following a new procedure.

The Megastat chamber also had to be properly cleaned before a cooldown. During the process of bringing the cryostat to vacuum, air pumped out of the system would cause debris inside of the chamber to land on the wafer surface. This problem could be remedied by pumping down to vacuum much slower, creating smaller air currents inside of the system that could blow flakes of Aquadag coating onto the wafer.

3.2   MCMC Development

3.2.1   View Factor Calculation

In previous models of the cryostat system, the geometric relationship between the test mass and the heat leaks had been approximated by two circular bodies on parallel planes (Figure 4). This created an upper bound for the amount of radiation leaking into the system that could be "seen" by the test mass, because a greater fraction of the radiation emitted from the test mass or heat leak could strike an incident plane that was parallel to a surface rather than horizontal. This upper bound could be improved by approximating the geometry of the cryostat system as the radiative heat transfer between two square bodies on perpendicular planes (Figure 4). In both cases, these approximations were used because the calculations for the view factors are very complicated, and the amount of time that it would take to calculate
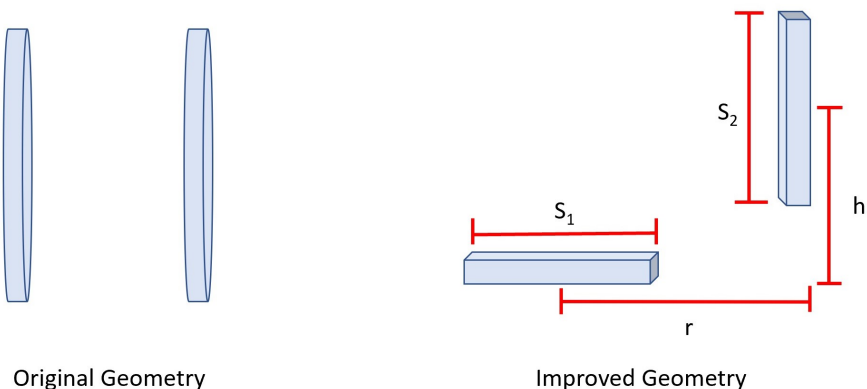
Figure 4: *Left:* The original model for the geometric view factor used geometry where the test mass and the heat leak were approximated as parallel to one another. This was done for simplicity and provided an upper bound to the view factor estimation. *Right:* The updated geometry is a function of the radius (r) between the center of the wafer and the effective heat leak and the height of the heat leak (h) relative to the test mass. S_1 and S_2 describe the side lengths of the wafer and the effective heat leaks if they are approximated as squares.

the exact shapes of the test mass and the heat leak are not worth the extra precision. Figure 4 shows the view factor calculation with respect to the test mass and a heat leak of effective side length. This approximation considers the heat leaks from both the RTD lead hole and the space around the cold bar (Figure 1), to be summed as an effective radius of a singular heat leak (Figure 5). This is assuming that the test mass is in the middle of the chamber and therefore that the heat leaks are all the same distance away from the test mass center. In practice, the test mass was not in the center of the chamber, although the difference in radii for each heat leak was most likely negligible.

3.2.2 MCMC on Silumated Data

Developing an MCMC script for analyzing cooldown data from the cryostat involved starting with a simple simulated model and building up to analyzing the real cryostat system.

The MCMC simulation was built up from Matt Pitkin's emcee python package linear model example [5]. This script estimated the parameters "m" and "b," describing the slope and y intercept of linear data simulated with Gaussian noise. This simulation took data and a model (in this case the model $y = mx + b$) as inputs and returned the posterior distributions for these data and priors. Figure 6 shows the corner plot for a run of this preliminary script where emcee recovered the parameters $m = 3.5$ and $b = 1.0$. MCMC was able to recover simulated parameters from data with some noise, and therefore it was possible to build this program up to a more complicated model with more parameters. This was a useful starting point because the simplicity of the model allowed for a better understanding of how the
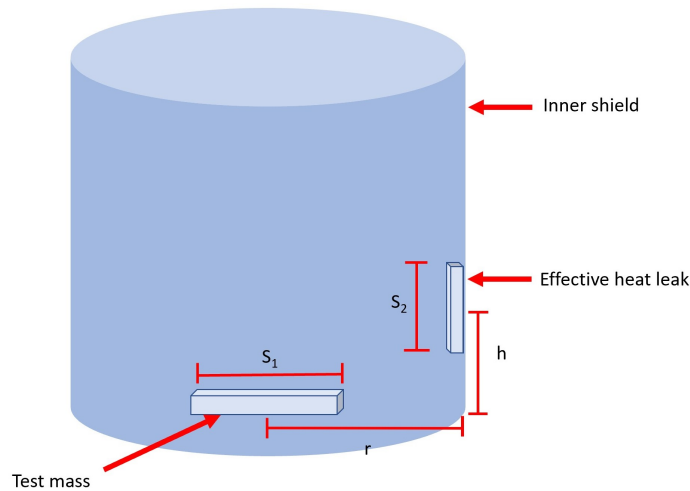
Figure 5: This shows a visualization of the view factor geometry in relation to the cryostat. The effective heat leak came from two points on the inner shield, and can be approximated as a square that is a radial distance away from the test mass.

emcee package worked and because it would later be necessary to treat the heat transfer differential equation as an algebraic model similar to the analysis for a linear model.

The next step in building emcee understanding was to simulate a parabolic model with three parameters. This simulation helped develop an understanding of how prior distributions effect the movement of walkers over the parameter vector space. Figure 7 shows the simulated data, trace plots, and corner plot for fitting a parabolic curve. These simple models provided the structure to build the more complex model for the cool down curve of the cryostat's test mass, as they gave an opportunity to encode more parameters into an algebraic model before moving to a differential equation.

One issue that effected the performance of the three-parameter MCMC was that the posterior distributions closely matched the prior distributions. This was evidence that the data was not providing new information to help inform the parameter estimations (the posterior should be proportional to the product of the likelihood and priors as in Equation 7). Because this analysis was conducted with simulated data with known parameters, the posterior plots that returned prior distributions was evidence of a bug in the code, not a fundamental problem with the model or data. This bug can be confirmed by passing uniform priors to the MCMC. Another good indication of how walkers are behaving is by looking at the trace plots. Walkers converge if they are able to find parameter vectors of highest likelihood. If the trace plots show walkers randomly exploring the parameter space and/or the posterior distributions are not forming a peak when they are supplied uniform priors, then that is indication that there is a bug in the emcee code or the model does not accurately represented by the data.

Finally, the parabolic model was edited to represent a simulated curve for radiative cooling and heating with added Gaussian noise, modeled by the equation
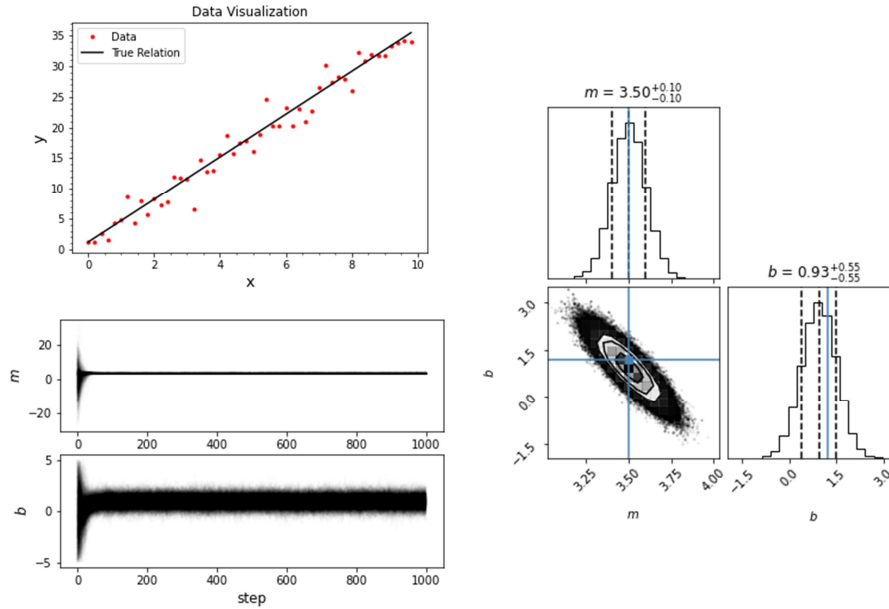
Figure 6: *Top Left:* The simulated data for the line $y = 3.5x + 1.0$ with Gaussian noise. *Bottom Left:* The trace plots for this model shows that both parameters converged well on a value. This is a useful way to check if the likelihood function is being maximized properly (refer to Section 2.2.2). *Right:* The corner plot for this analysis shows that the MCMC was able to estimate both parameters well, as evidence by the Gaussian posterior distributions. Notice the slanted angle of the combined distributions of the two parameters. This is indicative of large degeneracy between the variance in the values of the parameters. This is because the simulated data was generated from a model and then Gaussian noise was added on top of the simulation. The standard deviation in the posterior of b is much greater than the posterior of m because the variation in along the y axis is encoded within the parameter b.
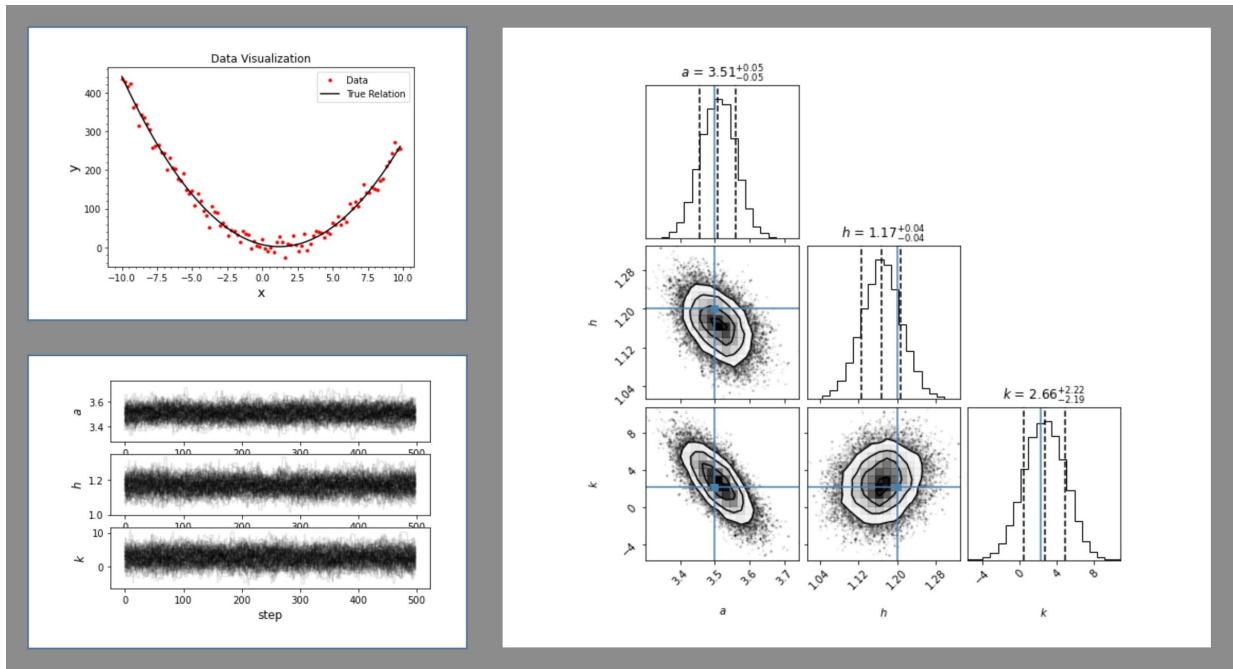
Figure 7: *Top Left:* The simulated data was a parabola with parameters in the form $y = a(x - h) + k$ with random noise, where $a = 3.5, h = 1.2$, and $k = 2.5$. *Bottom Left:* The majority of walkers were converging on a value and failed to "walk" around all areas of the valid parameter space. However, this alone is not an indication that the MCMC is working correctly, as there are ways to give the appearance of convergence through various bugs in the helper functions passed to emcee. *Right:* The generated corner plots provide information on the covariance between the parameters. It is also useful to see how the walkers converged. Notice that the posterior distribution for the parameter k has a wider standard deviation than the other parameters. This is because the random noise added to the data caused vertical shifts away from the theoretical line. The parameter k encodes how the parabola is shifted along the y axis. Therefore, the standard deviation for how well we can know this value will be greater.

$$mc_p \frac{dT_{tm}}{dt} = \frac{\sigma A_{tm}(T_{is}^4 - T_{tm}^4)}{\frac{1}{\epsilon_{tm}} + \frac{A_{tm}}{A_e}(\frac{1}{\epsilon_{is}} - 1)} + \frac{\sigma(T_{os}^4 - T_{tm}^4)}{\frac{1-\epsilon_{tm}}{A_{tm}\epsilon_{tm}} + \frac{1}{A_{tm}F_{tm->os}} + \frac{1-\epsilon_{os}}{A_{hl}\epsilon_{os}}}$$

(Equation 8). Figure 8 shows the simulated curve and numerically calculated derivative for those data. It is important to notice that this iteration of the code applied a numerical derivative with no smoothing, meaning that the derivative was very noisy. This code was changed to include smoothing in the numerical derivative calculation.
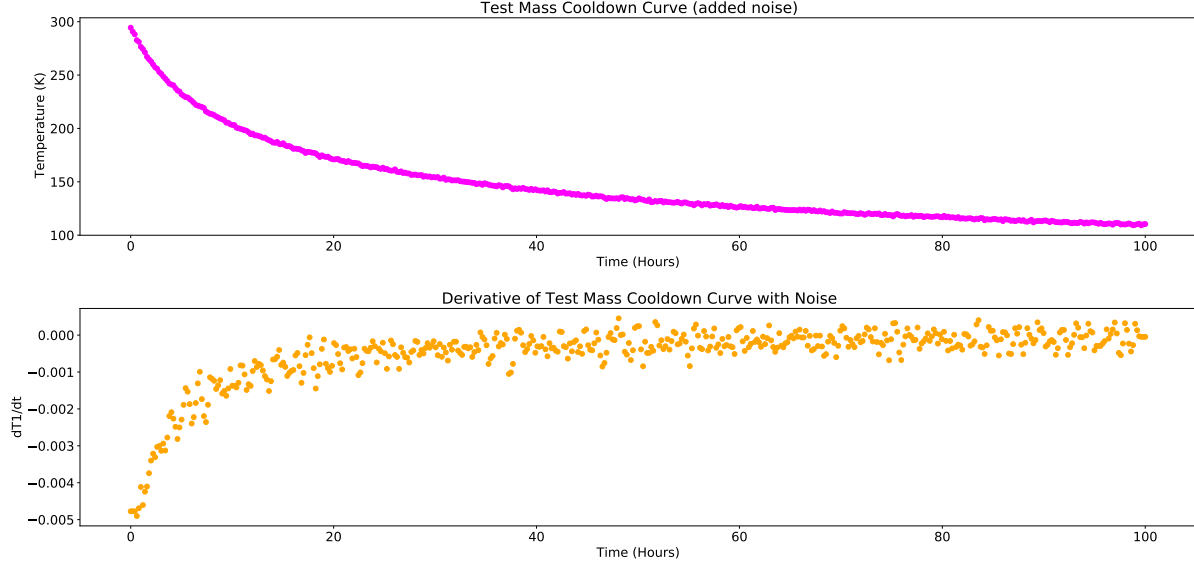
Figure 8: *Top:* The simulated data for a test mass cooldown describes a purely radiative cooling model. These data were simulated by first constructing a cooldown curve from known emissivities and then adding Gaussian noise. *Bottom:* The manually computed (unsmoothed) numerical derivative of the cooldown data. This derivative is very noisy compared to subsequent runs of the MCMC code.

Figure 9 shows how information from the data did not significantly contribute to the understanding of the posteriors by providing little information for the MCMC walkers. This is evident from observing how the walkers explored the prior space and how closely the prior distributions matched the posterior distributions. The walkers did not converge well and generally explored the entire region given in the prior, as evident in the trace plots in Figure 9. The posterior distributions almost perfectly matched the priors, meaning that the data were not providing enough information for MCMC to properly estimate new parameters. It is interesting to note that the posterior distributions for the emissivity of the inner shield and the heat leak (E2 and E3 respectively in Figure 9) moved in the opposite direction of the true value. This could be because the derivative of the cooldown curve was computed manually without any smoothing (Figure 8). This meant that the derivative data were very noisy, and could have effected how the MCMC found posterior distributions. When moving to real data, this issue was fixed by implementing a scipy smoothing method for computing the derivative to reduce noise. Another problem with the script was that the standard deviation of the numerical derivative was too big, meaning that the MCMC script was unable

to distinguish areas of higher likelihood because the likelihood helper function in the emcee code is dependent on the standard deviation of the data.
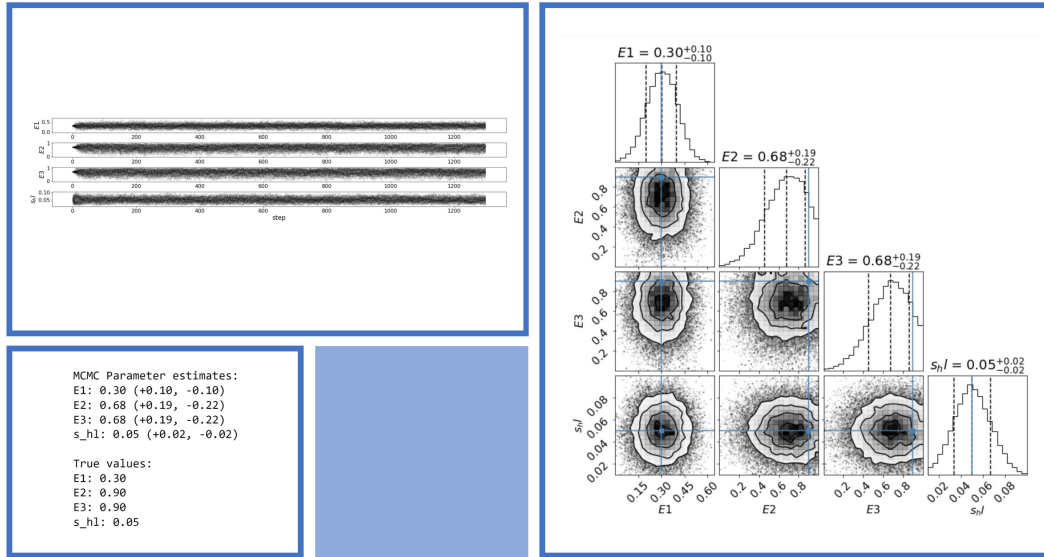

Figure 9: *Top Left:* The trace plots for the simulated data show the walkers exploring the whole parameter space. They did not converge well on a new value not given by the priors. *Bottom Left:* The true values of the emissivities and the heat leak aperture with uncertainty. This is an example of how it was useful to simulate data where we could recover known emissivities. *Right:* The corner plots for this run reveal that the posterior distributions are very similar to the prior distributions for the values where it was fed the correct priors. For the parameters where the prior distribution was off center from the real value, the posterior was slightly different. Interestingly, it moved in the opposite direction of the true value (refer to bottom left).

As a method to check if it was possible to fit for the individual emissivites due to observed degeneracy between ϵ_1 and ϵ_2 in the simplified model, a further simplified model was analyzed. When using a very simplified radiative model, it was found that there is no way to distinguish between the two parameters. This was further shown by using Scipy curve fit. Scipy curve fit could not recover the correct values of ϵ_1 and ϵ_2 without putting restrictions on the bounds of both parameters. This was a useful method to check if there was a problem with the way that emcee was finding the parameters or if there was no way for the values of these parameters to be distinguished without adding some restrictions to their values. The findings with scipy curve fit confirmed understanding of the degeneracy between the emissivity parameters when fitting a purely radiative model.

3.2.3   Algebraic to Differential Equation

The model for net heat transfer of a wafer in Megastat is dependent on a nonlinear differential equation. Although emcee can perform integration within each step of exploring the

parameter space, the temperature data for each cooldown along with the numerical derivative of the cooldown data was passed to MCMC so that the net heat transfer equation could be evaluated as an algebraic equation.

Ideally, the MCMC code would fit the differential equation to the temperature data by performing numerical integration. However, this is challenging to code when learning MCMC. Therefore, providing the data and the first derivative of the data was an intermediate step that directly linked the previous parabolic model to the ODE cooldown model. By providing both the data and it's first derivative, MCMC was estimating parameters the same way that it would for an algebraic equation by evaluating an array of 'x values,' or the cooldown data, and 'y values,' or the first derivative of the cooldown data.

This intermediate program numerically calculated the first derivative for each point on the simulated cooldown curve. The array of slopes and the simulated data were used to fit for the emissivities of the test mass, enclosure, and heat leak. The terms "enclosure" and "heat leak" refer to the inner and outer shield of the real system.

The original plan was to build a simulated cryostat and then make a simple change from the simulated data to real cooldown data. In theory, the only difference between the simulated script and the real cooldown script would be providing and interpolating the cooldown data for the inner and outer shields as functions of time. In the simulated models, the temperature of the inner and outer shields were approximated as constants. However, it became necessary to rewrite portions of the code from scratch because the model that most adequately represented Megastat was different from the simulated model because it required conductive terms.

3.2.4 MCMC on Cooldown Data

After developing simulated cooldowns of the cryostat system, a model for the cooldown of a silicon wafer was constructed. The simulated data script differed from the script used for real cooldowns because it was necessary to incorporate the cooldown timeseries for the inner and outer shields instead of approximating these values as constants. This is because the temperature of the inner and outer shields did not immediately drop to their equilibrium temperatures (Figure 10). It was also necessary to add conductive terms to the cooldown model and to refine the provided dimensions of Megastat. Using Equation 5, the emissivity of silicon, the effective side length of the heat leak, and the coefficients of the conductive heating and cooling terms were estimated in the July-11-2022 cooldown of a silicon wafer. Figure 11 shows the curve that the MCMC was fitting for, which can be integrated to recover the cooldown curve.

This analysis was run with both uniform and Gaussian priors. In the case of Gaussian priors, the prior distributions supplied were (in the form [mean, standard deviation]), $\epsilon_1 = [0.35, 1]$, side length of heat leak = [0.04, 0.013], $\alpha = [4, 4]$, $\beta = [4, 4]$. The priors on α and β were scaled by a factor of 1000 to make them visible on the corner plots. Because the are included purely for fitting purposes and not for providing information on the emissivity, the true values of the conductive coefficients do not matter and they can be left as arbitrary values.
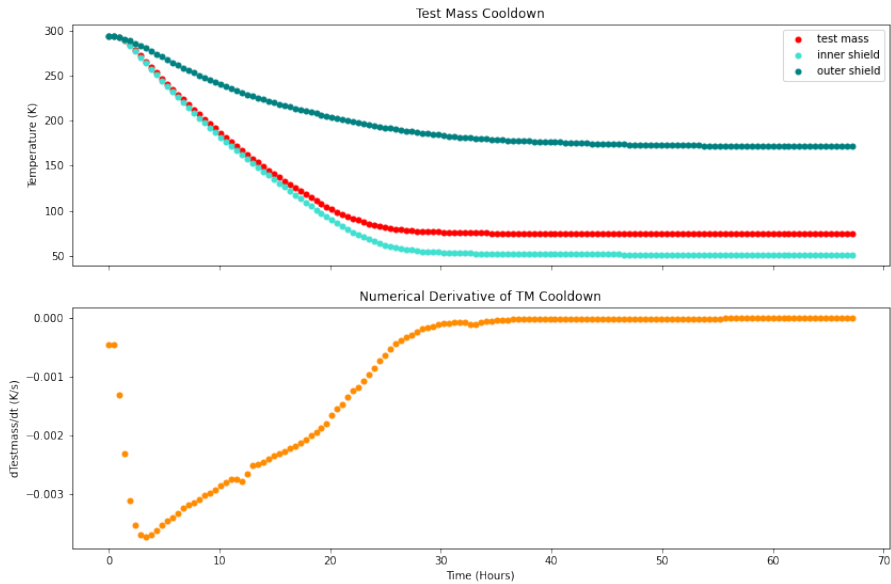
Figure 10: *Top*: The July-11-2022 cooldown timeseries for the inner shield, outer shield, and silicon test mass wafer. The test mass temperature stabilized between that of the inner and outer shield. This is because the inner shield is in conductive contact with the cold head, and therefore reached a colder equilibrium temperature than the outer shield, which is closer to the ambient temperature of the room. *Bottom*: The numerical derivative of the test mass cooldown with respect to time. This was obtained using the scipy.signal.savgol_filter method.
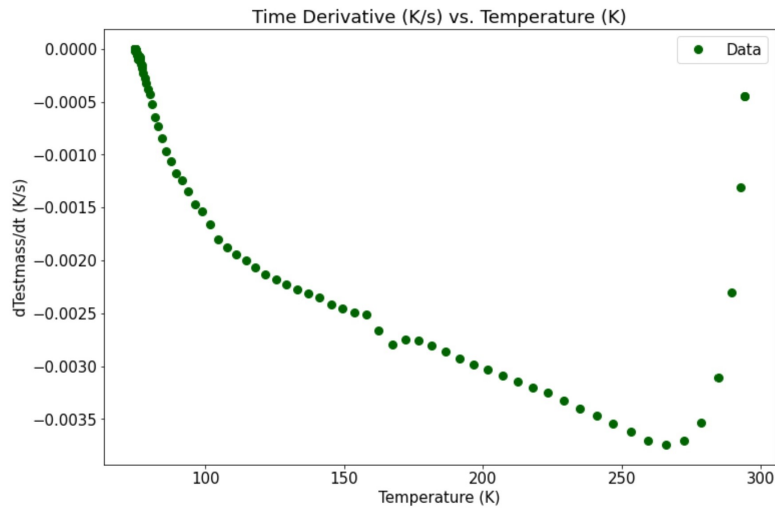
Figure 11: The numerical time derivative of the temperature data for the silicon wafer cooldown was plotted against the temperature. This is the curve that MCMC was fitting for as described in section 3.2.3.

The uniform prior for ϵ_1 was $[0, 1]$ because emissivity is a value strictly between zero and one. The uniform prior on the effective side length of the heat leak was decided based on what would be reasonable within Megastat. The bounds were $[0, .5]$ in units of meters. There is no physical way that the heat leaks would be larger than 50 cm, and there are clearly visible leaks, so the parameter value must be larger than zero.

It was also important to provide an estimate for the standard deviation of the derivative of the cooldown curve. MCMC was able to estimate the size of a heat leak as long as the standard deviation provided was within $+/-$ one order of magnitude of the true value. This meant that it is possible to make an educated guess on the standard deviation of the derivative of the cooldown curve. For the July-11-2022 data, the standard deviation was set to .001.

4   Results and Discussion

The emissivity of the silicon wafer used in the July-11-2022 cooldown was found to be $0.72 +/- .04$. Figure 12 shows the corner plot generated from the MCMC analysis of this cooldown.
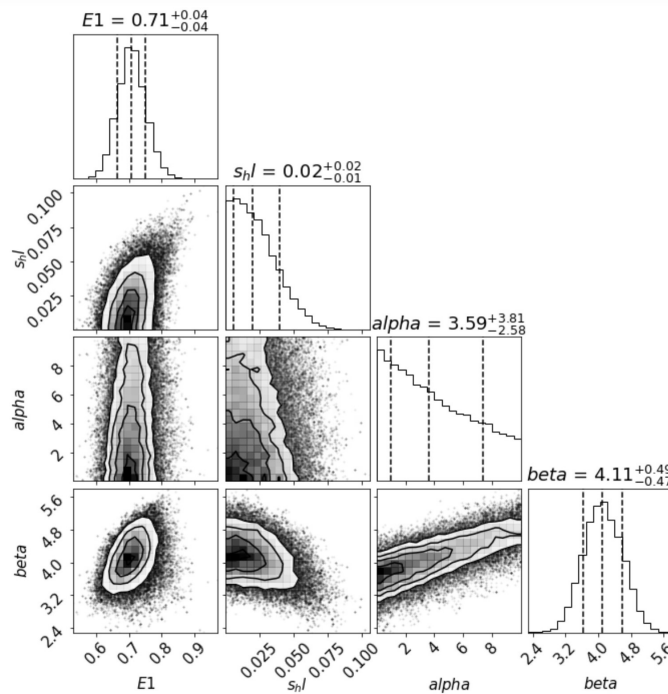

Figure 12: The corner plot fitting for the emissivity of the silicon wafer (E1), the size of the heat leak (s_hl), and the conductive heating (alpha) and cooling (beta) terms using uniform priors shows that the MCMC was able to find a value of ϵ_1 (E1) to high precision (5.6% accuracy). This analysis was run with uniform priors.

Although the emissivity of the inner shield and outer shield were not well known, it was not necessary to include parameters for their values in the MCMC fit. The posterior distributions for both parameters were uniform, indicating that the data did not inform a
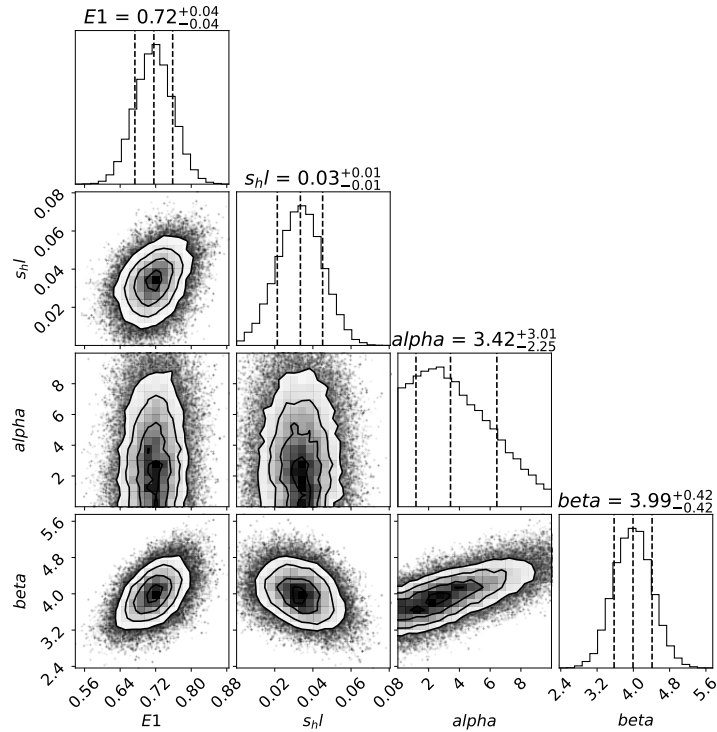
Figure 13: It was reasonable to run the MCMC using Gaussian priors because we could provide information on the size of the heat leak and emissivity of silicon. This analysis is identical to the analysis in Figure 11, except for the use of Gaussian priors. This corner plot shows the results of this analysis. Comparing to Figure 11, providing a Gaussian prior for the effective size of the heat leak did effect the estimation of ϵ_1. Using uniform priors, the emissivity estimation for the silicon wafer was $0.71 +/- .04$. This analysis estimated ϵ_1 to be $0.72 +/- .04$. This is 1.4% difference in the estimation by providing more information on the system.
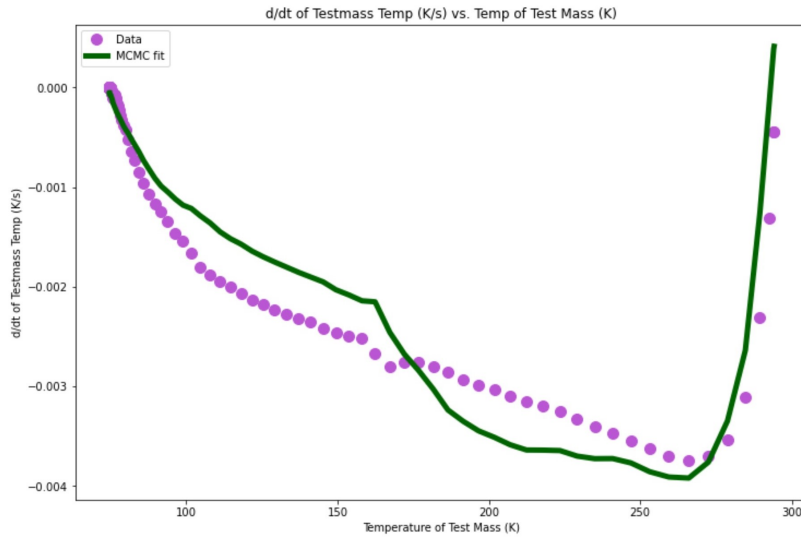
Figure 14: The MCMC fit for the numerical time derivative of the temperature data versus the temperature is the general shape of the data. This shape was only achieved once both conductive heating and cooling terms were added. Although this does not look like a good match to the data, integrating an comparing to the timeseries shows that MCMC was able to estimate the parameters of interest accurately (Figure 15).
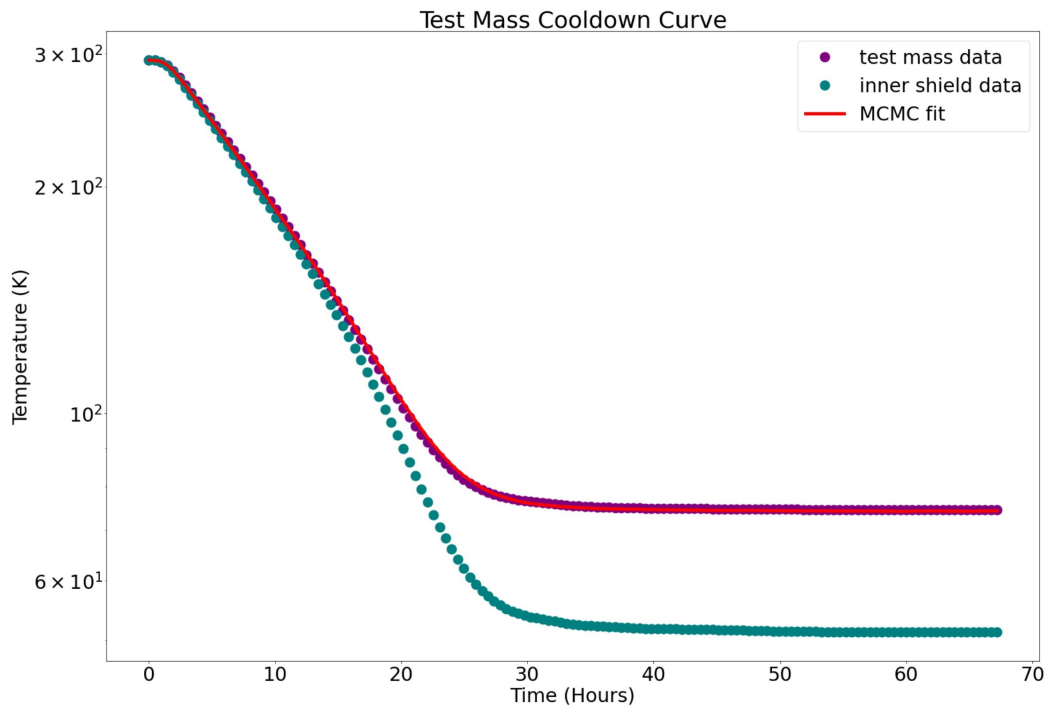

Figure 15: The fit in Figure 14 could be compared to the cooldown data by integrating with respect to time using the model and the estimated parameters. This gives a visual of how well the fit from Figure 14 matched the cooldown curve.

better understanding of their posterior distributions. For simplicity, these emissivities were hard-coded into the model with reasonable guesses (emissivity of inner shield = 0.8 due to high-emissivity coating and the emissivity of outer shield = 0.1). The fit did not significantly change based on whether these emissivites were given to MCMC as parameters. Knowing that the posterior distributions of the inner and outer shield emissivities were uniform informs how Megastat needs to be maintained and updated. This analysis shows that if the inner shield gets minor scrapes or damages, it can still be used for cooldowns. This is useful because the Aquadag coating flakes easily.

There was also discrepancy in the value of ϵ_1 (emissivity of the test mass) when using uniform versus Gaussian priors. There is a 1.4% difference between the estimated values of the test mass emissivity when supplying different priors (Figure 12, 13). The standard deviation of the Gaussian distributions for all of the variables except for the effective heat leak side length were wide enough that they were effectively flat over their domains. Therefore, the only parameter that we provided meaningful information for was the effective heat leak side length, where we estimated that the heat leak was approximately 4 cm. The MCMC analysis found the effective side length was $3.3 +/- 0.1$ cm, lower than the measured value that was still within the uncertainty. Therefore, when the MCMC was provided priors on the size of the heat leaks, it estimated a value that was still reasonable given observations Megastat. Based on the difference in the estimation of ϵ_1, it can be assumed that this added information allowed for a difference in the estimated value of the emissivity, although both values were within the uncertainty of each other. This means that in future cooldowns, it is beneficial to provide a reasonable guess (based on measurements of the cryostat) for the surface area of the heat leaks and therefore the effective side length. However, providing a prior for the size of the heat leaks will not change the value of the parameter estimation for ϵ_1 significantly.

radiative_enclosure_corner_linear.pdf

Figure 16: The corner plot for the linear emissivity model shows that the slope parameter was tending towards zero using uniform distributions. However, the MCMC was able to find an estimation for the y-intercept parameter of the emissivity more accurately, indicating that the linear emissivity can be modeled as $E1 = 0.0003T + 0.6314$, where T is the temperature of the wafer.

The July-11-2022 cooldown data was also used to model the emissivity of silicon as a linear function of temperature. It is known that emissivity is a temperature dependent value. However, including linear temperature dependent emissivity gave a worse fit over the cooldown timeseries than fitting for a constant emissivity. Figure 17 describes the integrated model using the estimated parameters given a linear model. Although it is nearly identical to the fit using a constant emissivity, the curve found by MCMC is slightly lower than the real data at long time scales. The value of the parameter m is very small, meaning that if we were to adopt the belief that the temperature dependent emissivity is linear, the slope of the line is very close to zero (Figure 16). However, this line is still a plausible temperature dependent emissivity function. The temperature dependent emissivity of silicon may be a nonlinear function because estimating for the linear fit parameters led to less agreement in the cooldown timeseries fit.

The script developed for estimating the emissivity of silicon can be applied to many cooldowns of different high emissivity coatings. Furthermore, using the results from this analysis can develop a more accurate procedure that can be implemented to find the emissivity of various high emissivity coatings to apply to the Mariner upgrade. This project will allow for a more streamlined system and procedure for taking measurements and operating the cryostat system. Using this information will help inform what aspects of the cryostat system are important to measure and where noise and error can be reduced in the Megastat system.
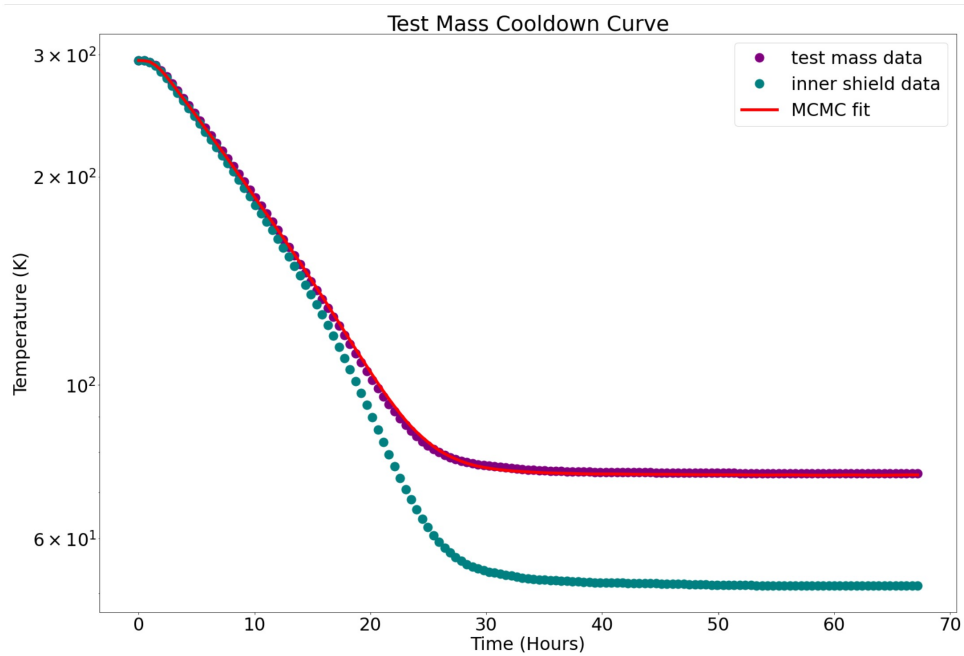
5   Acknowledgments

Figure 17: The linear emissivity fit did not provide as close agreement for the real timeseries after integration. Although it is a minor deviation, the MCMC fit stabilizes at a slightly lower value than the cooldown timeseries, which is barely visible on the logarithmic scale. This equilibrium is estimated more accurately using a constant emissivity parameter.

References

[1] V. Mitrofanov, *LIGO Voyager Project of Future Gravitational Wave Detector*, LIGO-G1602258-v2.

[2] M. Constancio and R. X. Adhikari and O. D. Aguiar and K. Arai and A. Markowitz and M. A. Okada and C. C. Wipf, International Journal of Heat and Mass Transfer, **157**, 2020.

[3] R. X Adhikari, A. Brooks, B. Shapiro, D. McClelland, E. K. Gustafson, V. Mitrofanov, K. Arai, C. Wipf, *LIGO Voyager Project of Future Gravitational Wave Detector*, LIGO-T1400226-v9.

[4] Y. A. Cengel, Heat transfer: a practical approach, McGraw-Hill series in mechanical engineering (McGraw-Hill, 2003) Chap. 12.

[5] M. Pitkin, An example using emcee, 2018, Accessed: 7-11-2022, Available: http://mattpitkin.github.io/samplers-demo/pages/emcee/

[6] I. Martinez, Radiative View Factors, (http://webserver.dmt.upm.es/ isidoro/tc3/Radiation %20View%20factors.pdf)

[7] Unknown Author, (http://www.fsb.miamioh.edu/lij14/400_slide_bs.pdf).

[8] The ideas for this report were based off of discussions with Professor Rana Adhikari (Experimental Gravitational Physics, LIGO Lab Caltech) and Radhika Bhatt (graduate student, Adhikari research group).